NeuroImage 331 (2026) 121882

Contents lists available at ScienceDirect

NeuroImage

journal homepage: www.elsevier.com/locate/ynimg

Technical Note

Harmonizing the stimulation dose of focal transcranial direct current stimulation across target sites

Axel Thielscher [a,b,*], Dayana Hayek [c], Oula Puonti [a,b], Ulrike Grittner [d,e], Felix Blankenburg [f,g], Rico Fischer [h], Gesa Hartwigsen [i,j], Shu-Chen Li [k,l], Marcus Meinzer [c], Michael A. Nitsche [m,n,o], Dagmar Timmann [p,q], Agnes Flöel [c,r], Daria Antonenko [c,**]

[a] Department of Health Technology, Technical University of Denmark, Kongens Lyngby, Denmark
[b] Danish Research Centre for Magnetic Resonance, Department of Radiology and Nuclear Medicine, Copenhagen University Hospital Amager and Hvidovre, Hvidovre, Denmark
[c] Department of Neurology, Universitätsmedizin Greifswald, Greifswald, Germany
[d] Berlin Institute of Health (BIH), 10187 Berlin, Germany
[e] Charité – Universitätsmedizin Berlin, Humboldt-Universität zu Berlin, Berlin Institute of Health, Institute of Biometry and Clinical Epidemiology, 10117 Berlin, Germany
[f] Neurocomputation and Neuroimaging Unit, Freie Universität Berlin, Berlin, Germany
[g] Berlin School of Mind and Brain, Humboldt-Universität zu Berlin, Berlin, Germany
[h] Department of Psychology, University of Greifswald, Greifswald, Germany
[i] Research Group Cognition and Plasticity, Max Planck Institute for Human Cognitive and Brain Sciences, Leipzig, Germany
[j] Wilhelm Wundt Institute for Psychology, Leipzig University, Leipzig, Germany
[k] Faculty of Psychology, Chair of Lifespan Developmental Neuroscience, TU Dresden, Dresden, Germany
[l] Centre for Tactile Internet With Human-in-the-Loop, TU Dresden, Dresden, Germany
[m] Leibniz Research Center for Working Environment and Human Factors, Dortmund, Germany
[n] Bielefeld University, University Hospital OWL, Protestant Hospital of Bethel Foundation, University Clinic of Psychiatry and Psychotherapy, Bielefeld, Germany
[o] German Center for Mental Health (DZPG), Bochum, Germany
[p] Department of Neurology, University Hospital Essen, University of Duisburg-Essen, Essen, Germany
[q] Center for Translational Neuro- & Behavioral Sciences (C-TNBS), University Duisburg Essen, Essen, Germany
[r] German Centre for Neurodegenerative Diseases (DZNE) Standort Greifswald, Greifswald, Germany

ARTICLE INFO

Keywords:
Non-invasive brain stimulation
Dose-response
Structural imaging
Simulation of electric fields
Computational modelling
Cognitive enhancement

ABSTRACT

Focal transcranial direct current stimulation (tDCS) using center-surround electrode montages enables region-specific cortical targeting, and holds promise for both cognitive neuroscience and clinical interventions. However, systematic examinations of dose-response relationships and their regional differences are lacking, hampering informed selections of suited stimulation parameters.

In this preparatory methodological study, we present a modeling-based framework to support harmonized empirical dose-response studies of focal tDCS across different target areas. It covers three steps: Determining the approximate electric field strength that had led to behavioral and physiological effects in related prior tDCS studies. In our case, this led to a field strength of 0.2 V/m on average across magnetic resonance images (MRIs) from 43 participants and eight target areas related to different cognitive and motor functions. Second, optimizing the radii of center-surround montages for each target area to - on average across participants - achieve the intended field strength while maximizing focality. An additional test of cross-sample generalization in an independent sample confirms that the intended target field strength is achieved on average for new participants. Third, the pre-determined montage radii and a method for the individualized positioning of the center-surround electrode montages are provided for prospective planning in empirical dose-response studies.

By harmonizing the electric field strength between different target regions at the group level, but preserving inter-individual variability, our framework will enable systematic analyses to relate the field strength to

* Corresponding author at: Department of Health Technology, Technical University of Denmark, Ørsteds Plads, Building 349,2800 Kgs. Lyngby, Denmark.
** Corresponding author at: Department of Neurology, University Medicine Greifswald, Ferdinand-Sauerbruch-Straße, 17475 Greifswald.
E-mail addresses: axthi@dtu.dk (A. Thielscher), dayana.hayek@med.uni-greifswald.de (D. Hayek), oupu@dtu.dk (O. Puonti), ulrike.grittner@charite.de (U. Grittner), felix.blankenburg@fu-berlin.de (F. Blankenburg), rico.fischer@uni-greifswald.de (R. Fischer), hartwigsen@cbs.mpg.de (G. Hartwigsen), shu-chen.li@tu-dresden.de (S.-C. Li), marcus.meinzer@med.uni-greifswald.de (M. Meinzer), nitsche@ifado.de (M.A. Nitsche), dagmar.timmann-braun@uk-essen.de (D. Timmann), agnes.floeel@med.uni-greifswald.de (A. Flöel), daria.antonenko@med.uni-greifswald.de (D. Antonenko).

https://doi.org/10.1016/j.neuroimage.2026.121882
Received 19 January 2026; Received in revised form 4 March 2026; Accepted 23 March 2026
Available online 24 March 2026

behavioral and neuroimaging outcomes, and to assess differences of these relations across regions. The described computational tools are open-source, allowing other researchers to tailor our framework to their specific research questions; and are currently used in a multi-center study involving approximately 1000 datasets.

1. Introduction

Transcranial direct current stimulation (tDCS) can modulate neural excitability and plasticity in target brain regions associated with specific cognitive, motor, or perceptual processes (Polanía et al., 2018). Considerable inter-individual variability in tDCS outcomes underscores the need to understand the factors driving these differences. Computational modeling suggests that individual differences in head and brain anatomy strongly influence how much current reaches the target region (e.g., Datta et al., 2009; Thielscher et al., 2015), resulting in substantial interindividual variability in the cortical dose. However, only few studies have investigated potential associations between the individually induced electric field strength and the corresponding modulation of brain activity, connectivity and behavior (Antonenko et al., 2017; Indahlastari et al., 2021; Jamil et al., 2020; Kim et al., 2014), with in part inconsistent results (Albizu et al., 2020; Antonenko et al., 2019; Liu et al., 2022; Mezger et al., 2021; Mosayebi-Samani et al., 2021; Muffel et al., 2019; Nandi et al., 2022). Thus, the relationship between electric field dose of tDCS and behavioral and neurophysiological outcomes, and the factors influencing this relationship (such as age or underlying brain microstructure), remains poorly understood. It is furthermore unclear how these relationships differ across brain regions and functional domains.

To address these open questions, we introduce a modeling-based framework to support harmonized empirical dose-response studies of tDCS across different target areas and functional domains. The framework preserves interindividual dose differences arising from anatomical variability within each target area, while harmonizing the *group-average* electric field dose across targets. This enables systematic tests of dose-response relationships and supports their comparison across areas and domains. We opted for focal tDCS center-surround montages, which allow region-specific targeting and minimize the unintended co-stimulation of surrounding areas (Alam et al., 2016; Kuo et al., 2013; Niemann, Shahbabaie, et al., 2024). Compared to conventional tDCS, focal tDCS montages may be better suited to investigate region-specific dose-response relationships, facilitating the distinction between local and remote network effects. To ensure comparable side effects across target regions, injected currents intensities were kept identical across montages. Harmonization of the group-average field dose was achieved by adjusting the center-surround electrode distances. These design constrains ruled out existing multi-electrode optimization approaches (Dmochowski et al., 2011; Radecke et al., 2020; Saturnino et al., 2020; Saturnino, Siebner, et al., 2019).

Our modeling-based framework consists of two main steps: First, for each functional domain of interest, we identified target areas and prior empirical studies reporting beneficial behavioral effects. We then simulated the electric fields of their electrode montages using magnetic resonance imaging (MRI) data from a group of participants (Sample 1). Averaging field magnitudes across participants and target areas yielded an empirically grounded target value of the electric field magnitude for subsequent montage optimization. This first step is needed because there is currently no general consensus regarding the minimal current intensity threshold required for physiological modulation and no knowledge about the potential optimization criteria for effective delivery (Fertonani and Miniussi, 2017; Lee et al., 2021). Second, we systematically varied the center-surround radii for each target region separately to identify the radius that achieved the intended target field magnitude on group-average in Sample 1. To ensure good spatial targeting and minimize unwanted co-stimulation, the center electrodes were thereby individually placed at skin positions with minimal Euclidean distance to the centers of the target regions. The selected radii were validated in an independent cohort (Sample 2) to confirm their generalizability to new participant groups, a critical requirement for their use in prospective planning. An additional control experiment confirmed that placement of the center electrode using the minimal Euclidean distance performed comparably to a more principled positioning approach that optimizes the electric resistance between the center electrode and the target region.

The determined region-specific radii and the individualized positioning method are currently used for the prospective planning in an ongoing multi-center study. However, the strategy is generic and the related code is available as open-source (https://github.com/simnibs/memoslap_utils), enabling adaptation to other target areas and stimulation parameters.

2. Methods

In the following, the initial Sections 2.1–2.5 provide general methodological details about the study populations, MR parameters and electric field simulations. Section 2.6 describes details for the first and second step of the framework, and Section 2.7 covers the third and fourth step. Section 2.8 describes the statistical analyses. Our modeling-based framework is illustrated in Fig. 1.

2.1. Participants

Structural brain images of 43 healthy adult participants (Sample 1, 23 females, age range: 20–47 years, mean/SD education: 16.6/2.1, all right-handed) were acquired to test our approach. To ensure reproducibility of estimated field magnitudes and focalities, we added a re-test dataset of 53 participants (Sample 2, 26 females, age range: 19–42 years, mean/SD education: 15.8/2.5, all right-handed). MR images of Sample 1 participants were acquired in the context of a study examining electrophysiological memory correlates and modulation. MR images of Sample 2 participants were acquired in the context of the multi-center project for which we aimed to develop the method. Exclusion criteria for participation in both studies were a history of neurological or psychiatric diseases, metal or electronic implants (e.g., pacemakers, surgical devices), and pregnancy. The studies were approved by the ethics committee of the Greifswald University Medicine and conducted in accordance with the Helsinki Declaration (Sample 1: BB 021/19; Sample 2: BB 015/22, 016/22, 017/22). Written informed consent was obtained from all participants prior to participation.

2.2. Magnetic resonance imaging

Sample 1 data were acquired on a 3T Siemens Verio equipped with a 32-channel head coil (Institute of Radiology, University Medicine Greifswald, Germany). High-resolution T1-weighted ($1 \times 1 \times 1$ mm^3, TR = 2300 ms, TE = 2.96 ms, TI = 900 ms, flip angle = 9°; using selective water excitation for fat suppression) and T2-weighted images ($1 \times 1 \times 1$ mm^3, TR = 12,770 ms, TE = 86 ms, flip angle = 111°) were recorded. Sample 2 data were acquired on a 3T Siemens Vida using a 64-channel head coil, high-resolution T1- ($0.9 \times 0.9 \times 0.9$ mm^3, TR = 2700 ms, TE = 3.7 ms, TI = 1090 ms, flip angle = 9°; using selective water excitation for fat suppression) and T2-weighted images ($0.9 \times 0.9 \times 0.9$ mm^3, TR = 2500 ms, TE = 349 ms) were recorded.

2.3. Head segmentation

Tissue segmentation of the head and brain from T1- and T2-weighted images was performed using charm from SimNIBS version 4.0 (simnibs.org) (Puonti et al., 2020; Thielscher et al., 2011). The generated individual tetrahedral head meshes including representations of the scalp, skull, spongy bone, compact bone, cerebrospinal fluid (CSF), gray matter, white matter, large blood vessels and eyes.

All electric field simulation results were interpolated onto the individual middle gray matter surfaces suited centrally between the pial and white matter surfaces for further analyses. The middle gray matter surfaces are automatically created by SimNIBS charm during head segmentation using embedded CAT12 (Gaser et al., 2024) functionality. In addition, to enable a consistent surface-based analysis approach also for target regions in the cerebellum, a surface that approximates the middle of the cerebellar gray matter was reconstructed from the volume segmentation results obtained by charm. This was done by assigning different isopotential values (0.0 and 1.0) to the boundaries between the segmented cerebellar gray matter and CSF, as well as between cerebellar gray and white matter. The Laplace equation was then solved to determine the isopotential surface for 0.5, indicating the middle positions between the two boundaries. Owing the limited image resolution of clinical structural MR images, the fine cortical folding structure of the cerebellum is not resolved in the volume segmentation and also not present in the reconstructed middle surfaces. The electric field estimates in the cerebellum thus only capture the impact of the gross cerebellar anatomy on the induced field. Individual datasets were visually inspected in order to assure accurate head reconstructions (Nielsen et al., 2018). All data were deemed appropriate.

2.4. Mapping of target regions-of-interest into subject space

All target regions-of-interest (ROI) were defined in group spaces (fsaverage or MNI). Group-level ROIs of the left and right hemispheres of the cerebrum were defined on fsaverage space, to leverage the higher accuracy of surface-based compared to volume-based registrations when transforming ROIs to the individual brain (Duecker et al., 2014). We also defined a cerebellar ROI, for which we used the MNI space. For each participant, the group-level ROIs of the left and right hemispheres of the cerebrum were mapped to the individual middle gray matter surfaces, applying the surface-based registration of CAT12 embedded in SimNIBS. The group-level ROI in the right cerebellar lobe was non-linearly transformed from MNI to individual space using SimNIBS functionality and intersected with the cerebellar middle gray matter surface. The resulting subject-specific ROIs were used to inform the subsequent field calculations and for calculating individual ROI sizes (in [mm^2]) using SimNIBS functionality.

2.5. Calculation of tissue volumes underneath the center electrodes

In order to test the relation between the electric field in the ROIs and individual anatomy, the volumes of CSF, skull (compact and spongy bone combined) and scalp were extracted in cylindrical volumes of interest underneath the center electrodes of the focal tDCS montages for cortical targets. The cylinders were oriented orthogonally to the local skin surface extracted from the tetrahedral head meshes, had radii of 20 mm and reached 40 mm into the head mesh. The tissue volumes in mm^3 were calculated by summing the volumes of the tissue-specific tetrahedra of the head mesh inside the cylinders.

2.6. Framework steps 1 and 2: simulation of electric fields for "empirical" electrode montages to determine the target field strength

For planning of the ongoing multi-center study, we identified eight target regions related to our functional domains of interest (step 1: target definition). We employed an iterative approach that considered both anatomical landmarks, previous task-related fMRI and transcranial direct current stimulation (tDCS) studies that have investigated the respective cognitive or motor function that are targeted in the eight projects (P1–8) of the multi-center study: P1, object-location learning; P2, tacto-spatial working memory; P3, novel-word learning; P4, verbal working memory; P5, motor sequence learning; P6, eyeblink

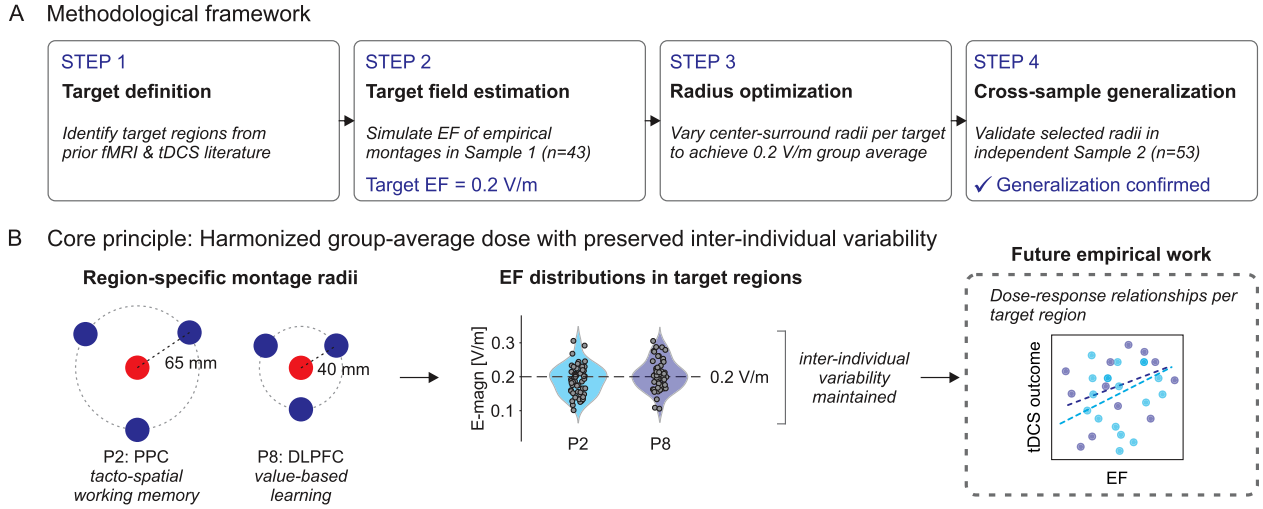

Fig. 1. Modeling-based framework for harmonized focal tDCS dose across target regions. (A) Methodological pipeline. The framework consists of four steps: (1) identification of target regions based on prior fMRI and tDCS literature; (2) simulation of electric fields (EF) of empirical tDCS montages in an initial participant sample (Sample 1, $n = 43$) to determine an empirically grounded target field strength. For the montages considered in our case, this related in of 0.2 V/m; (3) systematic variation of center-surround radii per target region to identify the radius achieving the intended group-average field magnitude; and (4) cross-sample generalization in an independent cohort (Sample 2, $n = 53$) to confirm that the selected radii achieve comparable group-average field strengths in new participants. (B) Core principle illustrated for two exemplary target regions (P2: tacto-spatial working memory; P8: value-based learning). Left: region-specific center-surround montages with different radii (P2: 65 mm; P8: 40 mm). Center: distributions of individually simulated EF values in each target region. Despite different montage radii, both regions achieve the same group-average field strength (0.2 V/m, dashed red line), while inter-individual variability in dose is preserved, a prerequisite for subsequent dose-response analyses. Right: the preserved inter-individual dose variability enables future correlational analyses of dose-response relationships per target region (hypothetical curves shown; not part of the present study).

conditioning; P7, learning-based control; P8, value-based learning. Atlas-based brain areas (Desikan et al., 2006) showing the highest overlap with the regions targeted in the empirical projects were determined as regions-of-interest (ROIs): P1, right occipitotemporal cortex (Gillis et al., 2016), P2, left superior parietal lobe (Schmidt et al., 2021; Wang et al., 2019), P3, left inferior frontal gyrus/pars opercularis (Filippova et al., 2022; Perceval et al., 2020; Perikova et al., 2022), P4, left inferior frontal gyrus/pars opercularis (Emch et al., 2019; Niu et al., 2019), P5, left primary motor/precentral cortex (Nitsche et al., 2003; Pimentel et al., 2013), P6, right cerebellar lobe (corresponding to Crus I and Lobule VI from the SUIT atlas (Diedrichsen and Zotow, 2015; Zuchowski et al., 2014)), P7, right dorsolateral prefrontal/rostral middle frontal cortex (Gbadeyan et al., 2016; Kerns et al., 2004), P8, left dorsolateral prefrontal/rostral middle frontal cortex (Eppinger et al., 2015; Nikolin et al., 2018). The resultant group-level ROIs were created by overlapping the atlas regions with spheres of 20-mm radius around the center of gravities of fMRI activity (except for P6 where the atlas-based ROI was used given its specific parcellation) to achieve more regional precision and corresponded to parts of the gyrus relevant for the respective cognitive/motor function.

Stimulation parameters were defined in SimNIBS corresponding to the actual setups in previous studies targeting the respective functional domains (Supplementary Figure 1 for illustration of electrode positions and Supplementary Table 1 for project and task details and Supplementary Table 2 for stimulation parameters). The standard tissue conductivity values of SimNIBS were used for the simulations. Median electric field strength (in V/m), averaged within the target ROI and field focality (quantified as area of field values above the median) were extracted from individual grey matter central surface outputs (step 2: target field estimation). Field strength (i.e., the vector norm of the electric field in V/m) within the ROIs was defined as target variable due to its independence from direction of the field and based on previous evidence for associations with anatomical features and empirical effects (Saturnino, Puonti, et al., 2019). The median field strength across all ROIs was used as target field strength for the subsequent optimization of the focal montages.

2.7. Framework steps 3 and 4: optimization of the focal tDCS montages

The optimization was performed for focal tDCS montages consisting of three surround electrodes distributed at equal angles around the center electrode. The present approach was developed specifically for focal tDCS using small electrodes in an Nx1 center-surround configuration, as our aim was to achieve spatially targeted (i.e., focal) stimulation of well-defined cortical regions, while maintaining practical feasibility using a low number of electrodes. All electrodes were simulated round with 2 cm diameter, and a current of 2 mA was injected in the center electrode that acted as anode.

The optimization consisted of two parts: First, placing the center electrode above the ROI center to optimize the focality-intensity tradeoff of the induced electric fields. This step was individualized to ensure that the induced fields are robustly centered on the individual ROIs. Second, reducing the radius of the montage as much as possible to minimize the co-stimulation of other areas while ensuring the desired field strength in the target. Of note, optimization of the radii in the second step was done on the group level, with the aim to achieve the same field strength in the different target regions on average across participants while preserving inter-individual variability. Correspondingly, in the latter empirical applications, only the montage positions but not the radii will be personalized.

We developed and compared two algorithms to position the electrode montage above a target ROI. One algorithm (termed "Euclidean optimization") minimizes the Euclidean distance of the center position on the scalp surface to the ROI centers. However, considering the complex head anatomy, the smallest Euclidean distance might not correspond to the scalp position that is electrically “best” connected to the ROI. Thus, the other algorithm (“resistivity optimization”) instead solves a Laplace equation using the finite element method (FEM) of SimNIBS, where the cortical ROI and the remaining cortex surface are set to different isopotential values (1.0 and 0.0). This choice corresponds to weighting all parts of the ROI equally as target and treating the rest of the brain surface homogeneously as avoidance region, which is the standard choice in “classical” optimization algorithms for multi-channel stimulation for optimizing focality (Dmochowski et al., 2017; Saturnino, Siebner, et al., 2019). The scalp position with the highest potential value is then chosen as center position. This ensures that the electric resistance between the center electrode and the ROI is chosen as small as possible relative to the resistance between the center electrode and the rest of the cortex. Both algorithms performed very similarly (see Results), confirming the suitability of algorithm 1 that was finally chosen as it was computationally more efficient and faster in practice. See also Supplementary Material B for further analyses to evaluate the performance of our approach.

For optimizing the montage radii (step 3: radius optimization), they were varied from 40 to 75 mm and simulated for each subject of sample 1 in 5 mm steps. For each ROI, the minimal center-surround radius was selected which ensured that the desired target field strength was on average reached while keeping the field as focal as possible. Finally, simulations with the selected radii were repeated in Sample 2 to validate that the intended target field strength was reached on group average also in an independent sample (step 4: cross-sample generalization).

We chose three instead of four surround electrodes due to practical feasibility. Note, however, that using more than three surround electrodes does not markedly change the field (Videira et al., 2022). We replicated this previous result in our analyses, showing nearly identical field magnitudes and focality in 4 × 1 and 3 × 1 montages (see Supplementary Figure 2 for an illustration of magnitude comparability). Orientation was varied for different angles (between 0 and 105° in 15°-steps). As the orientation of the cathodes did not systematically impact electric field magnitudes on the group level (Supplementary Figure 3), we selected a practically feasible phi-offset for each project (for instance, not covering the ears or eyes).

2.8. Statistical analyses

R was used for statistical analyses (R Core Team, 2020). Center-surround radii were determined on Sample 1 data while all further statistical comparisons were calculated on Sample 2 data. For each dependent variable, we conducted Cohen’s d to quantify the effect size of pairwise comparisons between projects, based on a linear mixed model approach. Cohen's d is a standardized metric that expresses the magnitude of the difference between two groups, accounting for the variability within each group. To calculate Cohen's d for each pairwise project comparison, we first estimated the model based marginal mean difference between the groups and then divided it by the pooled standard deviation of the measurements. This method allowed us to assess the observed differences between project performances, considering both the effect size and the variability inherent in the data in a standardized way. Linear mixed model analyses (random intercept models) were calculated for each dependent variable (magnitude or focality). Independent variables were the project (project 1 to 8), algorithm (1 or 2), age, and sex, with an interaction term between project and algorithm included to assess potential variations in the effect of algorithm across different projects. A random intercept term was included to account for the repeated measurements or nested structure of the data, where a subject represents the individual units of observation. To further investigate pairwise comparisons of project variances, we calculated the log-transformed coefficient of variation ratio (CVR) for each pair of projects. CVR was computed as the ratio of the coefficient of variation (CV) of the magnitude and focality between two projects.

3. Results

3.1. Target regions

The target regions for the eight projects of the multi-center study were delineated based on anatomical information as well as functional magnetic resonance imaging (fMRI) and tDCS studies, and are illustrated in Fig. 2A. We observed interindividual variability as well as differences between projects in ROI sizes with low values in project 1 (Cohen's d between 0.71 and 2.36; compared with projects 2, 3, 4, 5, 7, 8) and project 6 (Cohen's d between 1.01 and 2.6; compared with projects 2, 3, 4, 5, 7, 8) and high values for project 2 (Cohen's d between 0.86 and 2.6; compared with projects 1, 4, 5, 6, 7, 8) and high values in project 3 (Cohen's d between 0.72 and 1.58; compared with projects 1, 2, 5, 6; Supplementary Figure 4).

3.2. Target field strength

Using data of Sample 1, we simulated the field distribution for eight "empirical montages". We observed high variability of the average median electric field strength in the target ROIs across participants, with a range from 0.06 to 0.39 V/m across electrode montages (median (IQR) P1: 0.14 (0.03), P2: 0.28 (0.03), P3: 0.13 (0.02), P4: 0.25 (0.04), P5: 0.31 (0.05), P6: 0.21 (0.04), P7: 0.11 (0.03), P8: 0.14 (0.05); Supplementary Figure 5A) with large differences between projects (Supplementary Figure 5B). The overall average across projects was 0.20 V/m.

Focality values ranged between 0.10 to 9.96 dm^2 (median (IQR) P1: 2.29 (1.99), P2: 3.31 (1.19), P3: 0.65 (0.13), P4: 2.80 (0.70), P5: 1.91 (0.77), P6: 0.48 (0.41), P7: 0.27 (0.10), P8: 0.19 (0.09); Supplementary Figure 5C) with likewise large differences between projects (Supplementary Figure 5D).

Based on these simulations, we defined a field strength of 0.2 V/m as the "target field strength" to be reached over the study sample on average for each of the projects. Note, that this threshold resulted from averaging field magnitudes in all positions within the target region, which is lower than the peak dose. As substantial parts within the target areas exceed the threshold of 0.2 V/m, we additionally computed the 95th percentile in the target regions (Mirjalili et al., 2025). The results

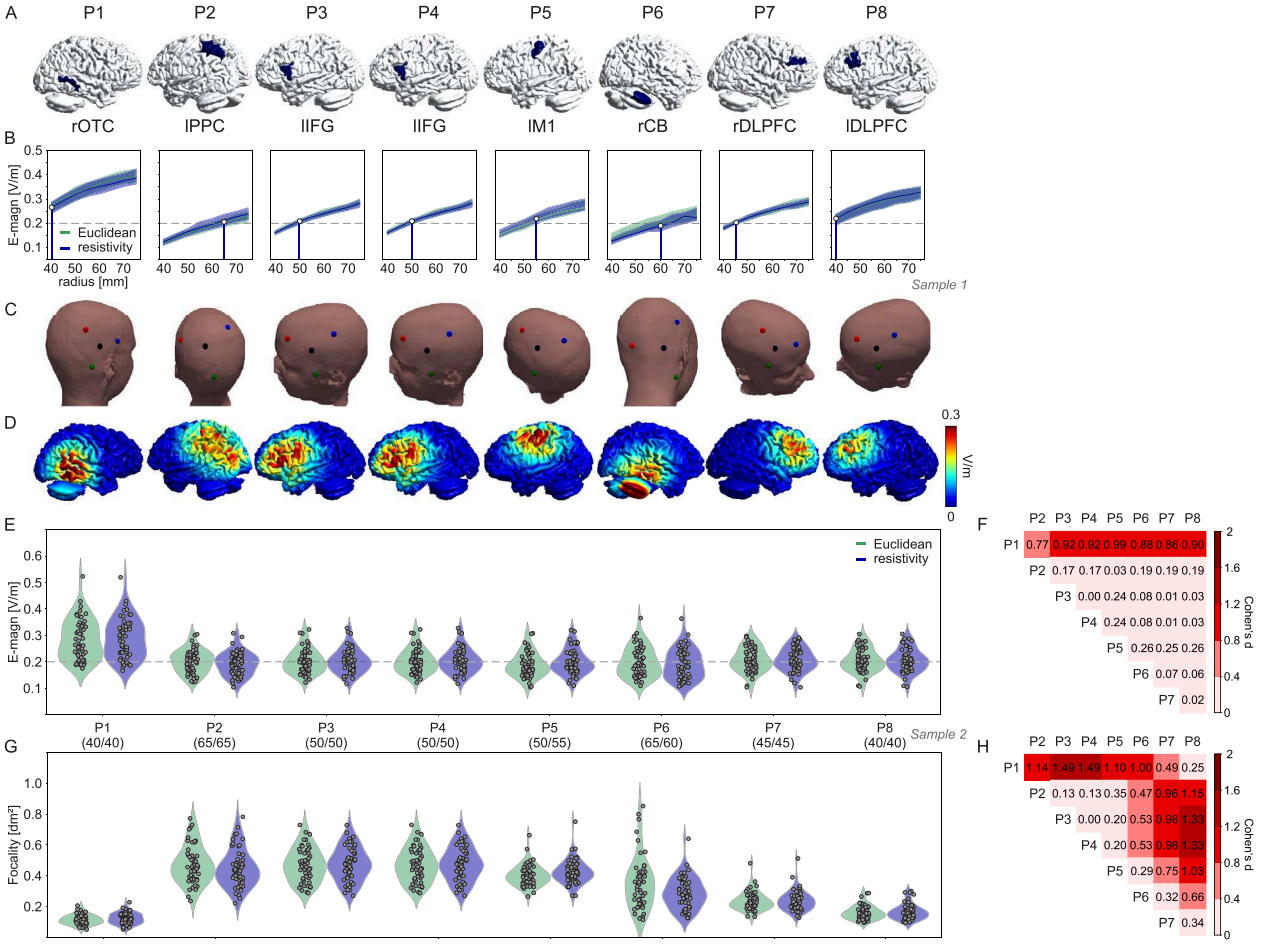

Fig. 2. (A) Target regions for individual projects of the research unit "MeMoSLAP" (eight projects P1–8: P1, object-location learning; P2, tacto-spatial working memory; P3, novel-word learning; P4, verbal working memory; P5, motor sequence learning; P6, eyeblink conditioning; P7, learning-based control; P8, value-based learning) illustrated for one subject from the sample. (B) Variation of distance between center anode and the three surround cathodes (Sample 1, $n = 43$). The dashed line represents the average electric field strength (0.2 V/m) that resulted from preparatory computational modeling analyses of "empirical" montages yielding beneficial tDCS effects. (C) Resultant electrode positions of the 3 × 1 focal tDCS set-ups for focal tDCS in P1–8 with matched average electric field magnitudes in target regions for the "Euclidean" algorithm. Note: while positions for the anodes were optimized for individual subjects, residual variability within studies will allow for testing cortical dose-relationships. (D) Sample e-field distributions for the given 3 × 1 set-ups. (E) Average electric field magnitude induced in target ROIs in 53 participants (Sample 2) with the resultant set-up for P1–8 (radii of Euclidean/resistivity algorithms in brackets). (F) Pairwise comparison of electric field magnitude between projects (Cohen's d; $n = 53$ subjects, number of obs: 848). (G) Focality of tDCS induced in target ROIs in 53 participants with the resultant set-up for P1–8. (H) Pairwise comparison of electric field focality between projects (Cohen's d; $n = 53$ subjects, number of obs: 848). rOTC, right occipitotemporal cortex. lPPC, left posterior parietal cortex. lTP, left temporoparietal. lIFG, left inferior frontal gyrus. lM1, left motor cortex. rCB, right cerebellum. rDLPFC/lDLPFC, right/left dorsolateral prefrontal cortex.

(Supplementary Figure 6) are in line with previously reported "effective doses" of 0.3 V/m (SD 0.11 V/m) for tACS (Alekseichuk et al., 2022) and for distinguishing responders from non-responders to tDCS (Mirjalili et al., 2025).

Further sensitivity analyses revealed: For a lower target field strength of 0.15 V/m, reducing the current intensity to 1.5 mA results in field strength-radius curves that are proportionally rescaled relative to the "0.2 V/m & 2 mA" set-up, with the optimized radii remaining unchanged. This is because the relationship between field strength and radius scales linearly with current intensity, such that the same montage geometry achieves the lower target value at the reduced intensity. For a higher target field strength of 0.3 V/m, we increased the current intensity to 2.5 mA, a value that remains within accepted safety and comfort limits for focal tDCS, and rescaled the individual field strength-radius curves accordingly by a factor of $2.5/2 = 1.25$. The optimized radii required to achieve 0.3 V/m at 2.5 mA were determined from the rescaled curves (Supplementary Figure 7). This analysis demonstrates that the proposed framework generalizes across a practically relevant range of target field strengths, provided that current intensity is adjusted proportionally. It also illustrates that selecting a too high target field strength at fixed current intensity would push the optimized radii toward the maximum feasible value, reducing focality, an important practical constraint that supports the choice of 0.2 V/m at 2 mA as the primary scenario in the present study.

3.3. Group-level optimization of center-surround radii for focal brain stimulation

Using simulations in Sample 1, the center-surround radii required for a median target field strength of 0.20 V/m were determined for each ROI, resulting in radii from 40 mm to 65 mm depending on the ROI. For confirmation, Fig. 2B shows the electric field magnitudes (averaged within the ROIs) of Sample 2 in dependence on the radii, demonstrating the determined radii achieve the intended target field strength also in an independent sample. Fig. 2C shows the electrode placements on a sample head, and Fig. 2D the related sample field distributions. Please note that the median field strength of P1 stayed higher than the desired target field strength even for the smallest radius of 40 mm. We did not reduce the radius further in order to maintain practical feasibility and prevent unintended shunting by electrode gel bridges.

The two algorithms for placing the center electrodes resulted in almost identical field magnitude estimations, warranting the "Euclidean optimization" as valid.

3.3.1. Magnitude

Individual electric field magnitudes within the target regions were all distributed around the target field strength of 0.2 V/m, except the occipitotemporal cortex (P1) where the group-based average lay above this threshold. Accordingly, a statistical comparison of electric field magnitudes revealed differences between projects with higher values for P1 compared to the others (all Cohen's $d \geq 0.77$, for all other pairwise comparisons Cohen's $d \leq 0.24$; Fig. 2E, Fig. 2F). Although ROI sizes were not associated with electric field magnitudes (overall $r = 0.25$, $p = 0.797$) or focality from the focal tDCS simulation (overall $r = 0.172$, all $p = 0.862$), this and the following group-level analyses were adjusted for ROI sized to account for differences.

Coefficient of variation (CV) of electric field magnitudes, which quantifies their spread relative to their mean and thus represents inter-individual variability, showed higher variability in P6 and lower variability in P1 compared to the other projects (Supplementary Figure 8A).

3.3.2. Focality

Focality of the induced electric fields differed between projects with substantially higher focality (corresponding to lower values) in P1 (range of Cohen's d: 1.00–1.49; compared with P2, P3, P4, P5, and P6), P7 (range of Cohen's d: 0.75–0.98; compared with P2, P3, P4, and P5) and P8 (range of Cohen's d: 0.66–1.33; compared with P2, P3, P4, P5, P6; Fig. 2G, Fig. 2H). Coefficient of variation of electric field focality showed some differences between projects (Supplementary Figure 8B).

3.3.3. Relation between field magnitude and local anatomy

To explore how potential head and brain anatomical differences between the target regions can affect electric fields, we compared different tissue volumes (i.e., skin, skull, CSF) below the center electrodes. Volumes differed between cortical targets for skin (Cohen's d's between 0.01 and 2.31) and skull (Cohen's d between 0.01 and 2.20). These analyses revealed that mainly CSF volumes were lower for the occipitotemporal cortex (target in P1) compared to the other target regions (Cohen's d: 0.91–3.13), confirming that anatomical factors that differ systematically may indeed affect the comparability between regions (Supplementary Figure 9). Larger CSF volume was associated with lower electric field magnitudes at target areas ($r_{rm} = -0.72$, $p < 0.001$; Supplementary Figure 10) and explained 70 % of their variance (adjusted for skin and skull volume).

4. Discussion

The current study presents the methodological development of a positioning planning approach for focal tDCS that harmonizes the stimulation dose across target sites using electric field simulations. This includes the estimation of an "effective" dose from previous studies, algorithm development for electrode positioning, determination of optimal region-specific center-surround radii of the focal montages, and validation in an independent sample. Our work presents a preparatory study to allow prospective region-specific positioning of electrodes in studies investigating the relationship between electric field dose and the resulting activity and performance modulation.

The present study demonstrates the cross-sample generalization and feasibility of the planning approach. By cross-sample generalization, we refer to the demonstration that the target field strength is expected to be achieved as a *group average* when applied in new participants, as supported by the cross-sample generalization results. By feasibility, we refer to the finding that adapting the montage radii while keeping all other stimulation parameters identical is sufficient to equalize the mean dose across different target regions. In addition, we demonstrate that the individualized electrode placement approach ensures focused stimulation of the intended target regions at the individual level.

The present study does not provide experimental confirmation of the behavioral effectiveness of the proposed montages, nor does it establish whether the selected field strength is optimal for inducing behavioral effects in each target region. Whether the harmonized dosing approach translates into more consistent behavioral outcomes across target regions, and whether meaningful dose-response relationships can be detected using this framework, remains to be demonstrated in empirical work. These questions are directly addressed by our ongoing multicenter study, which will provide experimental validation.

Our open-source tools (https://github.com/simnibs/memoslap_utils) allow researchers to easily tailor montages to their intended target regions and target field strength.

4.1. Target field strength

Currently, there are no established, evidence-based, region-specific electric field thresholds for different brain areas. No general consensus exists regarding the minimal current intensity threshold required for physiological modulation which may even differ between individuals (Fertonani and Miniussi, 2017; Van Hoornweder et al., 2025). Studies have shown that higher electric fields (e.g., 0.25 V/m in left DLPFC) can produce stronger working memory improvements for tDCS (Caulfield et al., 2022). Some studies have reported thresholds around 0.2 to 0.3 V/m for distinguishing tDCS responders from non-responders (Mirjalili et al., 2025). Similar field strength thresholds have been reported by

Alekseichuk et al. (2022) for inducing effects in awake/behaving mammals by tACS (mean ± SD across five studies: 0.23 ± 0.10 V/m). Together, previous evidence supports that our target of 0.2 V/m is within a physiologically relevant range (Mirjalili et al., 2025; Van Hoornweder et al., 2025). However, optimal thresholds for specific human brain regions remain undetermined.

Our approach used a uniform average "effective" target field strength across all target regions. We followed the rationale that real tDCS applied in previous studies, yielding beneficial effects for 1–2 mA, would inform the selection of an average electric field magnitude needed to be achieved. This is a pragmatic, evidence-based starting point that accounts for interregional differences in head and brain anatomy that systematically affect the induced field. However, several local factors including cortical network organization and neuron properties including cytoarchitecture are likely to affect the physiological response thresholds. Thus, by harmonizing the group-average field strength across target regions while keeping the interindividual variability of the field strength, our goal here was to provide the methodological basis for systematic comparisons of dose-response relationships across brain areas and related cognitive and motor domains. This systematic evaluation and comparison of minimal effective doses across regions is possible as our approach results in different electric field strengths in each participant depending on head and brain anatomy.

Importantly, the provided open-source code allows adaptation of the "desired" region-specific field strength. Our dedicated aim was to ensure that the montages induce similar, behaviorally effective electric field ranges in different target regions while being as focal as possible.

4.2. Precision stimulation

A reliable method for prospective planning of focal tDCS application considering optimized individual spatial targeting is currently not available. Electrode placements in focal tDCS most often rely on the 10–20 electroencephalographic system. Due to interindividual anatomical differences, this approach may result in inaccurate electrode positioning in individual participants, thereby introducing variable electric fields in the target region (Huang et al., 2017; Niemann, Riemann, et al., 2024; Opitz et al., 2018; Woods et al., 2015). Our approach ensures that the focal tDCS montages are accurately centered above the target regions, with neuronavigation being used to ensure that the planned electrode positions are reliable reached in practice (Niemann, Shahbabaie, et al., 2024). In addition, our approach allows validating electrode placement based on a simple minimization of the Euclidean distance to the brain target, using a more principled approach that accounts for the impact of the different tissue conductance on the current pathways in the head.

We propose that the selected target areas for focal tDCS serve as key nodes within the functional networks supporting the respective cognitive and motor domains. In this framework, focal tDCS applied during task performance is expected to modulate activity preferentially in regions that are engaged by the task, thereby indirectly influencing the broader network through activity-selective stimulation effects (Meinzer et al., 2024). Our rationale for using focal montages is that this approach enables a clearer distinction between direct and indirect stimulation effects and facilitates systematic investigation of dose-response relationships.

While extending the approach to conventional large pad electrodes was beyond the scope of the present work, the underlying principle is transferable in theory. The core idea, i.e., modulating field strength in the target region by adjusting inter-electrode distance, should generalize to conventional pad electrode configurations. Such an extension would require the user to specify, for each target region, a displacement axis along which one or both pad electrodes are shifted, analogous to the variation of center-surround radii in the present approach.

4.3. Limitations

Our work should not be interpreted without acknowledging its limitations. We here want to point out potentially varying distributions across anatomical positions and cohorts:

For the P1 montage, the average target field strength remained above 0.2 V/m even at the lowest practically feasible center-surround radius of 40 mm. Control analyses quantifying the volumes of scalp, skull, and CSF underneath the electrodes demonstrated that local anatomical factors differed systematically between the target positions. Mainly CSF volume, which was substantially lower above the occipitotemporal cortex. These differences may limit the effectiveness of our strategy, which aims to homogenize the induced field strengths across positions by solely adjusting the center-surround radii. However, we chose not to reduce the radius below 40 mm to maintain practical feasibility and avoid shunting between electrodes. This could also impact dose-response relationships, making it more challenging to compare P1 with the other projects. Although the mean field strength in the occipitotemporal cortex exceeds the intended target value, the distribution of individual field strengths still overlaps with those of the other target regions. While reducing the applied current intensity would have been a straightforward solution to lower the target field strength, we here opted against it to maintain a consistent current intensity across all projects, also aiming to keep the sensory side effects similar. Further, modeling of the detailed folding structure within the cerebellar ROI (P6) was lacking. The reconstructed surface is placed at half of the depth of the cerebellar gray matter in order to ensure that the average field strength in the ROI is close to the average field strength in the true, highly folded gray matter. However, as the area of the cerebellar gray matter is strongly underestimated by the surface, the reported focality values for the cerebellar ROI are too small.

As our study was part of preparatory work for a multi-center study, we selected the age range of participants based on its aims (https://osf.io/t37u2), ensuring that the determined montage radii are applicable to that target population. We expect our approach to be robust within the relatively narrow age range tested here, given that pronounced structural changes are more characteristic of older age groups (Hedden and Gabrieli, 2004). The results of the cross-sample generalization step support this rationale: highly comparable group-average target field strengths were achieved across both cohorts despite differences in sample composition, suggesting that the approach will generalize to the multi-center study sample as well. This will allow investigating age effects on stimulation outcomes, but may limit conclusions outside this age range. Importantly, our tool can be applied for other age groups as well. Both cohorts tested here consisted exclusively of healthy participants, in line with the goal of the ongoing multi-center study. The models therefore do not account for lesioned or anatomically atypical brains.

4.4. Conclusions

We developed a strategy for estimating an effective electric field strength based on previous functional imaging and behavioral studies comparing real and sham tDCS. We used the results to inform an approach that ensures accurate spatial targeting of focal brain stimulation and enables the harmonization of the induced electric field strength across different target regions. Here, we provide a methodological framework to allow prospective planning of region-specific tDCS application and enable systematic assessments of interindividual and interregional differences in tDCS dose-response profiles. Whether it proves behaviorally effective requires future studies and is currently being investigated in a multicenter study.

In the future, our approach could be complemented by electric-field-based meta-analytic methods (Wischnewski et al., 2021) to more rigorously confirm that stimulation of the selected target areas contributed substantially to the observed behavioral effects. Notably,

our target region for verbal working memory is consistent with the area identified by that meta-analytic approach for working memory, lending additional support to our target selection.

Funding

This work was supported by the German Research Foundation (project grants: Research Unit 5429/1 (467143400), FL 379/34-1, FL 379/35-1, FL 379/37-1, FL 379/22-1, FL 379/26-1, FI 1624/6-1, ME 3161/5-1, ME 3161/6-1, AN 1103/5-1, TH 1330/6-1, TH 1330/7-1, NI 683/17-1, HA 6314/10-1, TI 239/23-1, BL 977/4-1, LI 879/24-1, 497919823, AN 1103/4-1). AT was supported by the Lundbeck foundation (grant R313-2019-622). GH was supported by Lise Meitner Excellence funding from the Max Planck Society, and by the European Research Council (ERC-2021-COG 101043747). DA was supported by the Heisenberg Programme of the DFG (project number: 539593253). The funders played no role in study design, data collection, analysis and interpretation of data, or the writing of this manuscript.

Data availability

The underlying code for this study is available in GitHub and can be accessed via this link https://github.com/simnibs/memoslap_utils. The datasets analysed during the current study are not publicly available due to potential identifying information that could compromise participant privacy, but are available from the corresponding author on reasonable request.

CRediT authorship contribution statement

Axel Thielscher: Writing – review & editing, Writing – original draft, Software, Funding acquisition, Formal analysis, Conceptualization. **Dayana Hayek:** Visualization, Formal analysis. **Oula Puonti:** Software, Formal analysis. **Ulrike Grittner:** Visualization, Formal analysis. **Felix Blankenburg:** Writing – review & editing, Funding acquisition. **Rico Fischer:** Writing – review & editing, Funding acquisition. **Gesa Hartwigsen:** Writing – review & editing, Funding acquisition. **Shu-Chen Li:** Writing – review & editing, Funding acquisition. **Marcus Meinzer:** Writing – review & editing, Funding acquisition. **Michael A. Nitsche:** Writing – review & editing, Funding acquisition. **Dagmar Timmann:** Writing – review & editing, Funding acquisition. **Agnes Flöel:** Writing – review & editing, Funding acquisition. **Daria Antonenko:** Writing – review & editing, Writing – original draft, Visualization, Investigation, Funding acquisition, Formal analysis, Conceptualization.

Declaration of competing interest

The authors declare the following financial interests/personal relationships which may be considered as potential competing interests:

MAN is in the scientific advisory board of Neuroelectrics and Précis's. All other authors declare no financial or non-financial competing interests. If there are other authors, they declare that they have no known competing financial interests or personal relationships that could have appeared to influence the work reported in this paper.

Acknowledgments

This study was performed in the context of the multi-center study MeMoSLAP - "Modulation of brain networks for memory and learning by transcranial electrical brain stimulation: A systematic, lifespan approach" (Research Unit FOR 5429, funded by the German Research Foundation: Deutsche Forschungsgemeinschaft, DFG; https://osf.io/t37u2).

Supplementary materials

Supplementary material associated with this article can be found, in the online version, at doi:10.1016/j.neuroimage.2026.121882.

References

Alam, M., Truong, D.Q., Khadka, N., Bikson, M., 2016. Spatial and polarity precision of concentric high-definition transcranial direct current stimulation (HD-tDCS). Phys. Med. Biol. 61 (12), 4506. https://doi.org/10.1088/0031-9155/61/12/4506.

Albizu, A., Fang, R., Indahlastari, A., O'Shea, A., Stolte, S.E., See, K.B., Boutzoukas, E.M., Kraft, J.N., Nissim, N.R., Woods, A.J., 2020. Machine learning and individual variability in electric field characteristics predict tDCS treatment response. Brain Stimul. 13 (6), 1753–1764. https://doi.org/10.1016/j.brs.2020.10.001.

Alekseichuk, I., Wischnewski, M., Opitz, A., 2022. A minimum effective dose for (transcranial) alternating current stimulation. Brain Stimul. 15 (5), 1221–1222. https://doi.org/10.1016/j.brs.2022.08.018.

Antonenko, D., Schubert, F., Bohm, F., Ittermann, B., Aydin, S., Hayek, D., Grittner, U., Flöel, A., 2017. tDCS-induced modulation of GABA levels and resting-State functional connectivity in older adults. J. Neurosci. 37 (15), 4065–4073. https://doi.org/10.1523/jneurosci.0079-17.2017.

Antonenko, D., Thielscher, A., Saturnino, G.B., Aydin, S., Ittermann, B., Grittner, U., Flöel, A., 2019. Towards precise brain stimulation: is electric field simulation related to neuromodulation? Brain Stimul. 12 (5), 1159–1168. https://doi.org/10.1016/j.brs.2019.03.072.

Caulfield, K.A., Indahlastari, A., Nissim, N.R., Lopez, J.W., Fleischmann, H.H., Woods, A. J., George, M.S., 2022. Electric field strength from prefrontal transcranial direct current stimulation determines degree of working memory response: a potential application of reverse-calculation modeling? Neuromodulation. 25 (4), 578–587. https://doi.org/10.1111/ner.13342.

Datta, A., Bansal, V., Diaz, J., Patel, J., Reato, D., Bikson, M., 2009. Gyri-precise head model of transcranial direct current stimulation: improved spatial focality using a ring electrode versus conventional rectangular pad. Brain Stimul. 2 (4), 201–207. https://doi.org/10.1016/j.brs.2009.03.005.

Desikan, R.S., Segonne, F., Fischl, B., Quinn, B.T., Dickerson, B.C., Blacker, D., Buckner, R.L., Dale, A.M., Maguire, R.P., Hyman, B.T., Albert, M.S., Killiany, R.J., 2006. An automated labeling system for subdividing the human cerebral cortex on MRI scans into gyral based regions of interest. Neuroimage 31 (3), 968–980. https://doi.org/10.1016/j.neuroimage.2006.01.021.

Diedrichsen, J., Zotow, E., 2015. Surface-based display of volume-averaged cerebellar imaging data. PLoS. One 10 (7), e0133402. https://doi.org/10.1371/journal.pone.0133402.

Dmochowski, J.P., Datta, A., Bikson, M., Su, Y., Parra, L.C., 2011. Optimized multi-electrode stimulation increases focality and intensity at target. J. Neural Eng. 8 (4), 046011. https://doi.org/10.1088/1741-2560/8/4/046011.

Dmochowski, J.P., Koessler, L., Norcia, A.M., Bikson, M., Parra, L.C., 2017. Optimal use of EEG recordings to target active brain areas with transcranial electrical stimulation. Neuroimage 157, 69–80. https://doi.org/10.1016/j.neuroimage.2017.05.059.

Duecker, F., Frost, M.A., de Graaf, T.A., Graewe, B., Jacobs, C., Goebel, R., Sack, A.T., 2014. The cortex-based alignment approach to TMS coil positioning. J. Cogn. Neurosci. 26 (10), 2321–2329. https://doi.org/10.1162/jocn_a_00635.

Emch, M., von Bastian, C.C., Koch, K., 2019. Neural correlates of verbal working memory: an fMRI meta-analysis. Front. Hum. Neurosci. 13, 180. https://doi.org/10.3389/fnhum.2019.00180.

Eppinger, B., Heekeren, H.R., Li, S.C., 2015. Age-related prefrontal impairments implicate deficient prediction of future reward in older adults. Neurobiol. Aging 36 (8), 2380–2390. https://doi.org/10.1016/j.neurobiolaging.2015.04.010.

Fertonani, A., Miniussi, C., 2017. Transcranial electrical stimulation:what we know and do not know about mechanisms. Neuroscientist 23 (2), 109–123. https://doi.org/10.1177/1073858416631966.

Filippova, M.G., Perikova, E.I., Blagovechtchenski, E.D., Shcherbakova, O.V., Kirsanov, A.S., Shtyrov, Y.Y., 2022. The nonspecific positive actions of direct current transcranial electrical stimulation on novel word acquisition. Neurosci. Behav. Physiol. 52 (8), 1254–1257. https://doi.org/10.1007/s11055-023-01354-3.

Gaser, C., Dahnke, R., Thompson, P.M., Kurth, F., Luders, E., The Alzheimer's Disease Neuroimaging, I, 2024. CAT: a computational anatomy toolbox for the analysis of structural MRI data. Gigascience 13. https://doi.org/10.1093/gigascience/giae049.

Gbadeyan, O., McMahon, K., Steinhauser, M., Meinzer, M., 2016. Stimulation of dorsolateral prefrontal cortex enhances adaptive cognitive control: a high-definition transcranial direct current Stimulation study. J. Neurosci. 36 (50), 12530–12536. https://doi.org/10.1523/JNEUROSCI.2450-16.2016.

Gillis, M.M., Garcia, S., Hampstead, B.M., 2016. Working memory contributes to the encoding of object location associations: support for a 3-part model of object location memory. Behav. Brain Res. 311, 192–200. https://doi.org/10.1016/j.bbr.2016.05.037.

Hedden, T., Gabrieli, J.D., 2004. Insights into the ageing mind: a view from cognitive neuroscience. Nat. Rev. Neurosci. 5 (2), 87–96. https://doi.org/10.1038/nrn1323.

Huang, Y., Liu, A.A., Lafon, B., Friedman, D., Dayan, M., Wang, X., Bikson, M., Doyle, W. K., Devinsky, O., Parra, L.C., 2017. Measurements and models of electric fields in the in vivo human brain during transcranial electric stimulation. Elife 6. https://doi.org/10.7554/eLife.18834.

Indahlastari, A., Albizu, A., Kraft, J.N., O'Shea, A., Nissim, N.R., Dunn, A.L., Carballo, D., Gordon, M.P., Taank, S., Kahn, A.T., Hernandez, C., Zucker, W.M., Woods, A.J.,

2021. Individualized tDCS modeling predicts functional connectivity changes within the working memory network in older adults. Brain Stimul. 14 (5), 1205–1215. https://doi.org/10.1016/j.brs.2021.08.003.
Jamil, A., Batsikadze, G., Kuo, H.I., Meesen, R.L.J., Dechent, P., Paulus, W., Nitsche, M. A., 2020. Current intensity- and polarity-specific online and aftereffects of transcranial direct current stimulation: an fMRI study. Hum. Brain Mapp. 41 (6), 1644–1666. https://doi.org/10.1002/hbm.24901.
Kerns, J.G., Cohen, J.D., MacDonald 3rd, A.W., Cho, R.Y., Stenger, V.A., Carter, C.S., 2004. Anterior cingulate conflict monitoring and adjustments in control. Science (1979) 303 (5660), 1023–1026. https://doi.org/10.1126/science.1089910.
Kim, J.H., Kim, D.W., Chang, W.H., Kim, Y.H., Kim, K., Im, C.H., 2014. Inconsistent outcomes of transcranial direct current stimulation may originate from anatomical differences among individuals: electric field simulation using individual MRI data. Neurosci. Lett. 564, 6–10. https://doi.org/10.1016/j.neulet.2014.01.054.
Kuo, H.-I., Bikson, M., Datta, A., Minhas, P., Paulus, W., Kuo, M.-F., Nitsche, M.A., 2013. Comparing cortical plasticity induced by conventional and high-definition 4 × 1 ring tDCS: a neurophysiological study. Brain Stimulation: Basic, Translat. Clinic. Res. Neuromodul. 6 (4), 644–648. https://doi.org/10.1016/j.brs.2012.09.010.
Lee, J.S.A., Bestmann, S., Evans, C., 2021. A future of current flow modelling for transcranial electrical stimulation? Curr. Behav. Neurosci. Rep. 8 (4), 150–159. https://doi.org/10.1007/s40473-021-00238-5.
Liu, M.L., Karabanov, A.N., Piek, M., Petersen, E.T., Thielscher, A., Siebner, H.R., 2022. Short periods of bipolar anodal TDCS induce no instantaneous dose-dependent increase in cerebral blood flow in the targeted human motor cortex. Sci. Rep. 12 (1), 9580. https://doi.org/10.1038/s41598-022-13091-7.
Meinzer, M., Shahbabaie, A., Antonenko, D., Blankenburg, F., Fischer, R., Hartwigsen, G., Nitsche, M.A., Li, S.C., Thielscher, A., Timmann, D., Waltemath, D., Abdelmotaleb, M., Kocataş, H., Caisachana Guevara, L.M., Batsikadze, G., Grundei, M., Cunha, T., Hayek, D., Turker, S., Flöel, A., 2024. Investigating the neural mechanisms of transcranial direct current stimulation effects on human cognition: current issues and potential solutions. Front. Neurosci. 18, 1389651. https://doi.org/10.3389/fnins.2024.1389651.
Mezger, E., Rauchmann, B.S., Brunoni, A.R., Bulubas, L., Thielscher, A., Werle, J., Mortazavi, M., Karali, T., Stöcklein, S., Ertl-Wagner, B., Goerigk, S., Padberg, F., Keeser, D., 2021. Effects of bifrontal transcranial direct current stimulation on brain glutamate levels and resting state connectivity: multimodal MRI data for the cathodal stimulation site. Eur. Arch. Psychiatry Clin. Neurosci. 271 (1), 111–122. https://doi.org/10.1007/s00406-020-01177-0.
Mirjalili, M., Brooks, H., Ma, C., Lee, A., Bikson, M., Voineskos, A.N., Blumberger, D.M., Fischer, C.E., Flint, A.J., Herrmann, N., Kumar, S., Lanctôt, K., Mah, L., Mulsant, B. H., Pollock, B.G., Rajji, T.K., 2025. Impact of tDCS-induced electric fields on slowing cognitive decline in older adults with mild cognitive impairment or remitted major depressive disorder: an analysis of the PACt-MD randomized clinical trial. Biol. Psychiatry. https://doi.org/10.1016/j.biopsych.2025.09.020.
Mosayebi-Samani, M., Jamil, A., Salvador, R., Ruffini, G., Haueisen, J., Nitsche, M.A., 2021. The impact of individual electrical fields and anatomical factors on the neurophysiological outcomes of tDCS: a TMS-MEP and MRI study. Brain Stimul. 14 (2), 316–326. https://doi.org/10.1016/j.brs.2021.01.016.
Muffel, T., Kirsch, F., Shih, P.C., Kalloch, B., Schaumberg, S., Villringer, A., Sehm, B., 2019. Anodal transcranial direct current stimulation over S1 differentially modulates proprioceptive accuracy in young and old adults. Front. Aging Neurosci. 11, 264. https://doi.org/10.3389/fnagi.2019.00264.
Nandi, T., Puonti, O., Clarke, W.T., Nettekoven, C., Barron, H.C., Kolasinski, J., Hanayik, T., Hinson, E.L., Berrington, A., Bachtiar, V., Johnstone, A., Winkler, A.M., Thielscher, A., Johansen-Berg, H., Stagg, C.J., 2022. tDCS induced GABA change is associated with the simulated electric field in M1, an effect mediated by grey matter volume in the MRS voxel. Brain Stimul. 15 (5), 1153–1162. https://doi.org/10.1016/j.brs.2022.07.049.
Nielsen, J.D., Madsen, K.H., Puonti, O., Siebner, H.R., Bauer, C., Madsen, C.G., Saturnino, G.B., Thielscher, A., 2018. Automatic skull segmentation from MR images for realistic volume conductor models of the head: assessment of the state-of-the-art. Neuroimage 174, 587–598. https://doi.org/10.1016/j.neuroimage.2018.03.001.
Niemann, F., Riemann, S., Hubert, A.K., Antonenko, D., Thielscher, A., Martin, A.K., Unger, N., Flöel, A., Meinzer, M., 2024a. Electrode positioning errors reduce current dose for focal tDCS set-ups: evidence from individualized electric field mapping. Clin. Neurophysiol. 162, 201–209. https://doi.org/10.1016/j.clinph.2024.03.031.
Niemann, F., Shahbabaie, A., Paßmann, S., Riemann, S., Malinowski, R., Kocataş, H., Caisachana Guevara, L.M., Abdelmotaleb, M., Antonenko, D., Blankenburg, F., Fischer, R., Hartwigsen, G., Li, S.C., Nitsche, M.A., Thielscher, A., Timmann, D., Fromm, A., Hayek, D., Hubert, A.K., Meinzer, M., 2024b. Neuronavigated focalized transcranial direct current stimulation administered during functional Magnetic resonance imaging. J. Vis. Exp. (213). https://doi.org/10.3791/67155.
Nikolin, S., Lauf, S., Loo, C.K., Martin, D., 2018. Effects of high-definition transcranial direct current stimulation (HD-tDCS) of the intraparietal sulcus and dorsolateral prefrontal cortex on working memory and divided attention. Front. Integr. Neurosci. 12, 64. https://doi.org/10.3389/fnint.2018.00064.
Nitsche, M.A., Schauenburg, A., Lang, N., Liebetanz, D., Exner, C., Paulus, W., Tergau, F., 2003. Facilitation of implicit motor learning by weak transcranial direct current stimulation of the primary motor cortex in the human. J. Cogn. Neurosci. 15 (4), 619–626. https://doi.org/10.1162/089892903321662994.
Niu, X., Li, J., Browne, G.J., Li, D., Cao, Q., Liu, X., Wang, G., Wang, P., 2019. Transcranial stimulation over right inferior frontal gyrus increases the weight given to private information during sequential decision-making. Soc. Cogn. Affect. Neurosci. 14 (1), 59–71. https://doi.org/10.1093/scan/nsy106.
Opitz, A., Yeagle, E., Thielscher, A., Schroeder, C., Mehta, A.D., Milham, M.P., 2018. On the importance of precise electrode placement for targeted transcranial electric stimulation. Neuroimage 181, 560–567. https://doi.org/10.1016/j.neuroimage.2018.07.027.
Perceval, G., Martin, A.K., Copland, D.A., Laine, M., Meinzer, M., 2020. Multisession transcranial direct current stimulation facilitates verbal learning and memory consolidation in young and older adults. Brain Lang. 205, 104788. https://doi.org/10.1016/j.bandl.2020.104788.
Perikova, E., Blagovechtchenski, E., Filippova, M., Shcherbakova, O., Kirsanov, A., Shtyrov, Y., 2022. Anodal tDCS over Broca's area improves fast mapping and explicit encoding of novel vocabulary. Neuropsychologia 168, 108156. https://doi.org/10.1016/j.neuropsychologia.2022.108156.
Pimentel, M.A., Vilela, P., Sousa, I., Figueiredo, P., 2013. Localization of the hand motor area by arterial spin labeling and blood oxygen level-dependent functional magnetic resonance imaging. Hum. Brain Mapp. 34 (1), 96–108. https://doi.org/10.1002/hbm.21418.
Polanía, R., Nitsche, M.A., Ruff, C.C., 2018. Studying and modifying brain function with non-invasive brain stimulation. Nat. Neurosci. 21 (2), 174–187. https://doi.org/10.1038/s41593-017-0054-4.
Puonti, O., Van Leemput, K., Saturnino, G.B., Siebner, H.R., Madsen, K.H., Thielscher, A., 2020. Accurate and robust whole-head segmentation from magnetic resonance images for individualized head modeling. Neuroimage 219, 117044. https://doi.org/10.1016/j.neuroimage.2020.117044.
R Core Team, 2020. R: a language and environment for statistical computing. R Foundation for Statistical Computing. https://www.R-project.org/.
Radecke, J.O., Khan, A., Engel, A.K., Wolters, C.H., Schneider, T.R., 2020. Individual targeting increases control over inter-Individual variability in simulated transcranial electric fields. IEEe Access. 8, 182610–182624. https://doi.org/10.1109/access.2020.3028618.
Saturnino, G.B., Madsen, K.H., Thielscher, A., 2020. Optimizing the electric field strength in multiple targets for multichannel transcranial electric stimulation. J. Neural Eng. https://doi.org/10.1088/1741-2552/abca15.
Saturnino, G.B., Puonti, O., Nielsen, J.D., Antonenko, D., Madsen, K.H., Thielscher, A., 2019a. SimNIBS 2.1: a comprehensive pipeline for individualized electric field modelling for transcranial brain stimulation. In: Makarov, S., Horner, M., Noetscher, G. (Eds.), Brain and Human Body Modeling: Computational Human Modeling at EMBC 2018. Springer, pp. 3–25. https://doi.org/10.1007/978-3-030-21293-3_1.
Saturnino, G.B., Siebner, H.R., Thielscher, A., Madsen, K.H., 2019b. Accessibility of cortical regions to focal TES: dependence on spatial position, safety, and practical constraints. Neuroimage 203, 116183. https://doi.org/10.1016/j.neuroimage.2019.116183.
Schmidt, T.T., Schröder, P., Reinhardt, P., Blankenburg, F., 2021. Rehearsal of tactile working memory: premotor cortex recruits two dissociable neuronal content representations. Hum. Brain Mapp. 42 (1), 245–258. https://doi.org/10.1002/hbm.25220.
Thielscher, A., Antunes, A., Saturnino, G.B., 2015. Field modeling for transcranial magnetic stimulation: a useful tool to understand the physiological effects of TMS? Conf. Proc. IEEe Eng. Med. Biol. Soc. 2015, 222–225. https://doi.org/10.1109/embc.2015.7318340.
Thielscher, A., Opitz, A., Windhoff, M., 2011. Impact of the gyral geometry on the electric field induced by transcranial magnetic stimulation. Neuroimage 54 (1), 234–243. https://doi.org/10.1016/j.neuroimage.2010.07.061.
Van Hoornweder, S., Stagg, C.J., Wischnewski, M., 2025. Personalizing transcranial electrical stimulation. Trends. Neurosci. 48 (9), 663–678. https://doi.org/10.1016/j.tins.2025.07.007.
Videira, A.S., Canadas, D., De, O.P.L., Andrade, A., Ferreira, H.A., Miranda, P.C., Fernandes, S.R., 2022. How the number and distance of electrodes change the induced electric field in the cortex during multichannel tDCS. Annu Int. Conf. IEEe Eng. Med. Biol. Soc. 2022, 2357–2360. https://doi.org/10.1109/EMBC48229.2022.9871114.
Wang, S., Itthipuripat, S., Ku, Y., 2019. Electrical stimulation over Human posterior parietal cortex selectively enhances the capacity of visual short-term memory. J. Neurosci. 39 (3), 528–536. https://doi.org/10.1523/JNEUROSCI.1959-18.2018.
Wischnewski, M., Mantell, K.E., Opitz, A., 2021. Identifying regions in prefrontal cortex related to working memory improvement: A novel meta-analytic method using electric field modeling. Neurosci. Biobehav. Rev. 130, 147–161. https://doi.org/10.1016/j.neubiorev.2021.08.017.
Woods, A.J., Bryant, V., Sacchetti, D., Gervits, F., Hamilton, R., 2015. Effects of electrode drift in transcranial direct current stimulation. Brain Stimul. 8 (3), 515–519. https://doi.org/10.1016/j.brs.2014.12.007.
Zuchowski, M.L., Timmann, D., Gerwig, M., 2014. Acquisition of conditioned eyeblink responses is modulated by cerebellar tDCS. Brain Stimul. 7 (4), 525–531. https://doi.org/10.1016/j.brs.2014.03.010.